


Crystal field splitting, local anisotropy, and low-energy excitations in the quantum magnet YbCl₃G. Sala¹, M. B. Stone¹, Binod K. Rai², A. F. May², D. S. Parker², Gábor B. Halász², Y. Q. Cheng¹, G. Ehlers³, V. O. Garlea¹, Q. Zhang¹, M. D. Lumsden¹, and A. D. Christianson^{2,*}¹Neutron Scattering Division, Oak Ridge National Laboratory, Oak Ridge, Tennessee 37831, USA²Materials Science & Technology Division, Oak Ridge National Laboratory, Oak Ridge, Tennessee 37831, USA³Neutron Technologies Division, Oak Ridge National Laboratory, Oak Ridge, Tennessee 37831, USA (Received 23 July 2019; revised manuscript received 2 November 2019; published 19 November 2019)

We study the correlated quantum magnet YbCl₃ with neutron scattering, magnetic susceptibility, and heat capacity measurements. The crystal field Hamiltonian is determined through simultaneous refinements of the inelastic neutron scattering and magnetization data. The ground-state doublet is well isolated from the other crystal field levels and results in an effective spin-1/2 system with local easy plane anisotropy at low temperature. Cold neutron spectroscopy shows low-energy excitations peaked at 0.5 meV that are consistent with nearest-neighbor antiferromagnetic correlations.

DOI: [10.1103/PhysRevB.100.180406](https://doi.org/10.1103/PhysRevB.100.180406)

The quantum spin liquid (QSL) is a state of matter hosting exotic fractionalized excitations and long-range entanglement between spins with potential applications for quantum computing [1–4]. Since QSL physics relies on quantum fluctuations that are enhanced by low spin and low dimensionality, spin-1/2 systems on two-dimensional lattices provide a natural experimental platform for realizing a QSL phase. It has also been shown that an *effective* spin-1/2 system can be generated even in compounds with high-angular-momentum ions such as Yb³⁺ and Er³⁺, where the combination of crystal field effects and strong spin-orbit coupling often yields highly anisotropic interactions between effective spin-1/2 degrees of freedom [5–7].

Magnetic frustration plays a central role in stabilizing QSL phases [8]. While QSLs were traditionally associated with geometrically frustrated systems (e.g., triangular and kagome lattices), it has recently become well appreciated that *exchange frustration* due to highly anisotropic spin interactions can also stabilize QSL phases, even on bipartite lattices [9,10]. Most famously, bond-dependent spin interactions on the honeycomb lattice give rise to the Kitaev model, an exactly solvable model with a gapless QSL ground state [11]. A number of honeycomb materials, primarily containing 4*d* or 5*d* transition metals such as Ru or Ir, have been put forth as realizations of the Kitaev model [12,13]. Prominent examples include (Na, Li)₂IrO₃ [14–21] and H₃LiIr₂O₆ [22], as well as α -RuCl₃ [23–36].

Recently, YbCl₃ has been proposed as a candidate material for Kitaev physics on a honeycomb lattice [37,38]. YbCl₃ crystallizes in the monoclinic space group *C*12/*m*1 (No. 12). The crystal structure is composed of layers of Yb³⁺ ions coordinated by slightly distorted Cl octahedra as illustrated in Fig. 1. Despite being formally monoclinic at 10 K, the Yb-Yb distances of 3.864 and 3.886 Å and the Cl-Yb-Cl bond angles of 96.12° and 96.73° are nearly identical [39]. The

results of this atomic arrangement are well-separated, nearly perfect honeycomb layers of Yb³⁺ ions in the *ab* plane as shown in Figs. 1(a) and 1(c). The environment surrounding the Yb³⁺ cations depicted in Fig. 1(b) consists of six Cl⁻ anions arranged in distorted octahedra where the *b* axis (\hat{y} axis) is the unique *C*₂ axis. Xing *et al.* [37] have reported that YbCl₃ undergoes short-range magnetic ordering at 1.2 K. A small peak in the heat capacity/temperature at 0.6 K may indicate a transition to long-range magnetic order. On the other hand, Yb-based quantum magnets have been the subject of recent investigations and, surprisingly, in some cases these materials have been found to possess strong effective Heisenberg exchange interactions [40–45]. Indeed, Ref. [46] predicts this to be the case for YbCl₃. Thus, key open questions for YbCl₃ are the nature of the spin Hamiltonian and the role of potential Kitaev terms. It is likewise important to determine the single-ion ground state out of which the collective physics grows and additionally if the ground-state doublet is well isolated and can be considered to be in the effective quantum spin-1/2 limit. In this Rapid Communication we study the single-ion physics through inelastic neutron scattering (INS) and thermodynamic measurements. We also study the low-energy excitation spectrum to determine the spin-spin correlations as an initial step towards understanding the spin Hamiltonian governing the physical behavior of YbCl₃.

Anhydrous beads of YbCl₃ and LuCl₃ were purchased from Alfa Aesar and utilized in the experimental work presented here. Additional information and results of sample characterization are provided in the Supplemental Material (SM) [39]. Refinements of neutron powder diffraction data did not reveal any significant chlorine deficiency or secondary phases [39].

The crystal field (CF) excitations were measured with INS performed with the SEQUOIA spectrometer at the Spallation Neutron Source at Oak Ridge National Laboratory (ORNL) [47]. Approximately 4.2 g of polycrystalline YbCl₃ and 2.5 g of its nonmagnetic equivalent LuCl₃ were loaded into cylindrical Al cans and sealed under helium exchange gas. The

*christiansad@ornl.gov

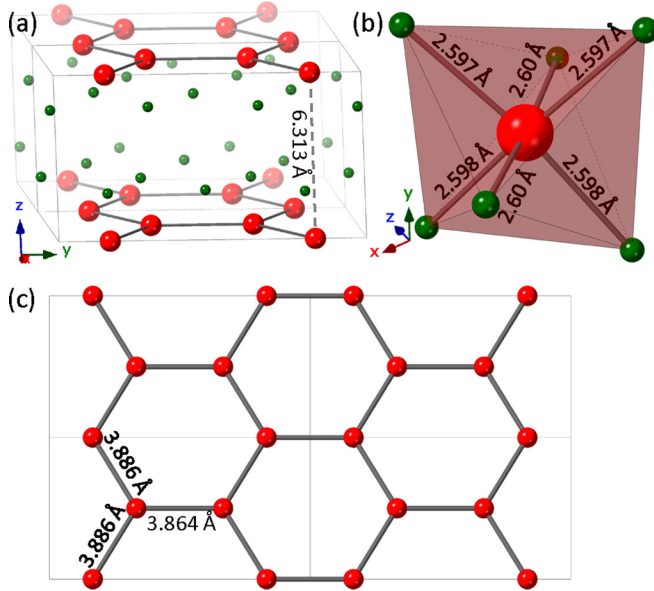


FIG. 1. Monoclinic crystal structure of YbCl_3 with $a = 6.7291(3)$ Å (\hat{x} axis), $b = 11.6141(9)$ Å (\hat{y} axis), $c = 6.3129(3)$ Å, and $\beta = 110.5997(7)^\circ$ obtained at 10 K. Refined structure parameters are further described in the SM [39]. (a) YbCl_3 structure consisting of alternating planes of Yb^{3+} cations (red spheres) forming a honeycomb lattice in the ab plane, with Cl^- anions (green spheres) separating the layers. (b) The crystal field environment surrounding the rare-earth ions consists of six Cl ions arranged in a distorted octahedron with C_2 point group symmetry. Note in this panel the octahedron has been rotated to coincide with that used for the crystal field modeling where the \hat{y} axis is the axis of quantization (the \hat{z} axis in the rotated coordinate system). (c) Single layer of Yb ions showing the honeycomb lattice in the monoclinic ab plane with Yb-Yb distances at 10 K.

use of the LuCl_3 measurement as a background subtraction is described in the SM [39]. The samples and an empty can for Al background subtraction [48] were measured at $T = 5, 95,$ and 185 K, with incident energies, $E_i = 6, 45,$ and 60 meV with the high-resolution chopper. The inelastic data presented here have had the measured backgrounds subtracted and data reduced using the software packages DAVE [49] and MANTID [50].

Figures 2(a) and 2(b) show the INS spectra as a function of wave-vector transfer Q and energy transfer $\hbar\omega$ measured at $T = 5$ and 95 K, respectively. Figure 2(c) is the wave-vector integrated scattering intensity from the $E_i = 60$ meV measurements for $2.5 \leq Q \leq 3.5$ Å $^{-1}$. The prominent higher-energy modes are identified as CF excitations both from their Q dependence and from comparison with the nonmagnetic analog LuCl_3 [39]. At $T = 5$ K they are centered at energy transfers of $\hbar\omega = 21.04, 32.03,$ and 39.28 meV. Increasing temperature reduces intensity but does not appreciably shift or broaden these transitions, consistent with the behavior expected for CF excitations. Note there are some low-energy phonon modes in the data that are not well subtracted, particularly near 4 meV.

To understand the nature of the CF spectrum, we analyze the energy levels following a formalism described by

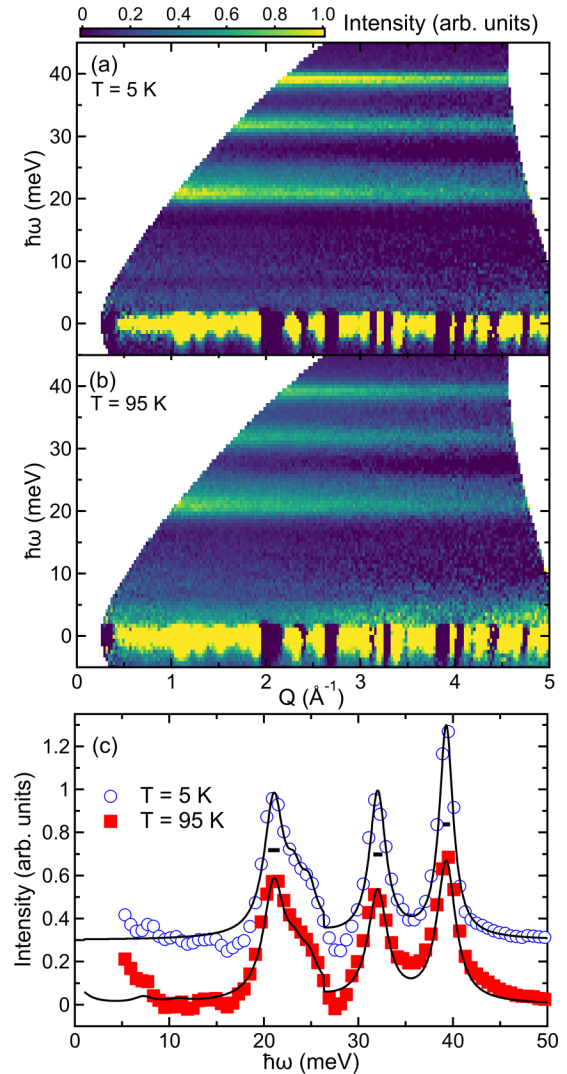


FIG. 2. Dynamic structure factor $S(|Q|, \hbar\omega)$ of YbCl_3 collected with SEQUOIA with $E_i = 60$ meV at (a) $T = 5$ K and (b) $T = 95$ K. The nonmagnetic background determined from LuCl_3 has been subtracted. Crystal field excitations are visible at $\hbar\omega = 21.04, 32.03,$ and 39.28 meV. (c) Comparison of the intensity of the CF transitions at $T = 5$ K and $T = 95$ K for YbCl_3 , in the momentum transfer range $Q = [2.5, 3.5]$ Å $^{-1}$. The solid lines are the results of the CF analysis using Eq. (1). Horizontal black lines denote instrumental resolution. The $T = 5$ K data and model are offset by 0.3 units along the vertical axis. The data are scaled so that the strongest CF level has an intensity of 1.

Wybourne [51–53] and Stevens [54]. Given the C_2 site symmetry of the local Yb environment, the CF Hamiltonian consists of 14 parameters [55]. Prather’s convention [56] for the minimal number of CF parameters was achieved by rotating the environment by $\pi/2$ around the a axis (\hat{x} axis), i.e., the axis of quantization becomes the b axis (the \hat{z} axis in the rotated coordinate system). To constrain the parameters, we simultaneously fit the neutron scattering data at 5 and 95 K between 15 and 45 meV [Fig. 2(c)], the magnetic susceptibility between 10 and 700 K (Fig. 3), and the field-dependent magnetization at 10 K (inset of Fig. 3).

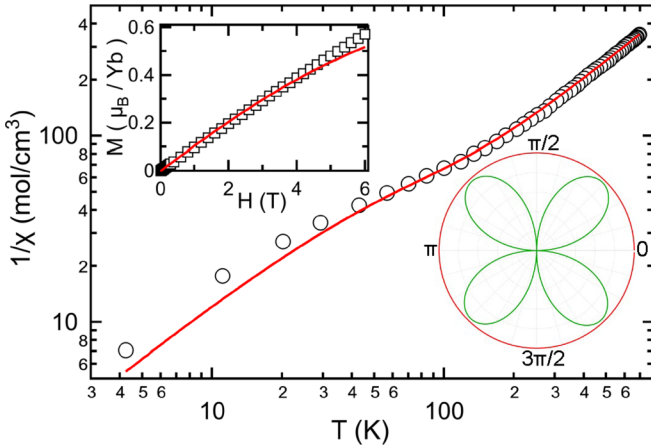


FIG. 3. Top: Inverse magnetic susceptibility χ as a function of temperature for polycrystalline YbCl_3 in the range $4 \leq T \leq 700$ K shown on a log-log scale for $H = 1T$. The red line is the result of a simultaneous fit of the CF model to the INS data (Fig. 2), the magnetic susceptibility, and the magnetization at 10 K. The top inset shows the calculated magnetization at 10 K compared with the experimental data. The bottom inset shows the calculated torque diagram using the CF parameters (green curve) at 2.1 K under an applied field of $5T$ (red circle) in the ab plane as measured in Ref. [37].

Hund's rules state that, for a $4f^{13}$ ion, $L = 3$ and $S = 1/2$, thus $J = \|L + S\| = 7/2$ [57]. Therefore the CF Hamiltonian can be written in terms of Steven's operators as

$$H = \sum_{n=2}^6 \sum_{m=0}^{\leq n} B_n^m \hat{O}_n^m + \sum_{n=4}^6 \sum_{m=2}^{\leq n} B(i)_n^m \hat{O}(i)_n^m \quad (1)$$

for n even, where B_n^m are the CF parameters, and \hat{O}_n^m are the Steven's operators [58] both in real and imaginary (i) form. Diagonalizing Eq. (1), the scattering function $S(|Q|, \hbar\omega)$ can be written as

$$S(|Q|, \hbar\omega) \propto \sum_{i,i'} \frac{(\sum_{\alpha} | \langle i | J_{\alpha} | i' \rangle |^2) e^{-\beta E_i}}{\sum_j e^{-\beta E_j}} L(\Delta E + \hbar\omega, \Gamma_{i,i'}), \quad (2)$$

where $\beta = 1/k_B T$, $\alpha = x, y, z$, $\Delta E = E_i - E_{i'}$, and $L(\Delta E + \hbar\omega, \Gamma_{i,i'})$ is a Lorentzian function¹ with half width $\Gamma_{i,i'}$ that parametrizes the line shape of the transitions between CF levels [eigenfunctions of Eq. (1)] $i \rightarrow i'$. We calculate the scattering function using this formalism, accounting for the Yb^{3+} magnetic form factor, and compare these values with the experimental data, and then vary the CF parameters to minimize the χ^2 difference between the model and the data shown in Figs. 2(c) and 3.

Point charge calculations were used to determine the starting parameters for the refinement of the CF Hamiltonian. Once convergence was achieved additional refinement loops were run where the CF parameters were varied to check that

TABLE I. Refined CF parameters in units of meV determined as described in the text. Each coefficient is presented divided by the corresponding Steven's parameter α_J , β_J , and γ_J [58].

B_2^0	B_2^2	B_4^0	B_4^2	B_4^4
-3.145	-27.347	5.623	39.845	-36.900
B_6^0	B_6^2	B_6^4	B_6^6	
-3.158	10.389	8.004	55.813	
$B(i)_4^2$	$B(i)_4^4$	$B(i)_6^2$	$B(i)_6^4$	$B(i)_6^6$
-6.29×10^{-3}	-9.89×10^{-3}	6.45×10^{-3}	-0.062	-0.028

the solution was not a local minimum. The refinement of the Hamiltonian [Eq. (1)] in the scattering function described in Eq. (2) yields the CF parameters presented in Table I and the set of eigenfunctions written in Table II of the SM [39]. The ground-state eigenfunctions are found to be

$$\pm 0.697 | \pm \frac{7}{2} \rangle \mp 0.341 | \mp \frac{5}{2} \rangle \pm 0.538 | \pm \frac{3}{2} \rangle \mp 0.328 | \mp \frac{1}{2} \rangle. \quad (3)$$

The imaginary part of the eigenfunctions is not shown because it is ≈ 2 orders of magnitude smaller than the real part. The calculated $S(|Q|, \hbar\omega)$ is plotted at both temperatures and shown in Fig. 2(c) as solid lines. The integrated intensity of the three CF excitations is reproduced as is the magnetic susceptibility (Fig. 3) and the field-dependent magnetization at 10 K (inset of Fig. 3).

The CF model demonstrates that the Yb^{3+} ions have a planar anisotropy and a calculated magnetic moment of $2.24(5)\mu_B/\text{Yb}$ is obtained for the ground state. The calculated components of the g -tensor for the ground-state doublet, using the convention described above, for YbCl_3 are $g_z = 4.09(2)$, $g_x = 3.96(2)$, and $g_y = 2.04(2)$, which shows somewhat more anisotropy than Ref. [37]. Additionally, using the CF model derived here as a starting point, we calculated a magnetic torque diagram at 2.1 K for an applied field of 5 T (Fig. 3 inset). The result reproduces the data in Ref. [37] (note the difference in coordinate conventions), demonstrating that the CF ground state is anisotropic independent of any additional exchange anisotropy.

Despite the overall quality of the fits, one aspect of the CF excitation spectrum remains puzzling. The line shape of the CF excitation centered at 21 meV extends toward higher energies. A similar broadening is not observed for the other CF excitations. Thus the broadening is a characteristic of the level at 21 meV and not of the ground state. To fully account for the spectral weight, we have modeled the line shape for this excitation as two constrained Lorentzians with the widths fixed to be the same and the positions offset by a fixed amount. The lack of observable impurity peaks in the neutron diffraction data [39] suggests that this effect is not due to an impurity phase. Deviations from ideal Cl stoichiometry are similarly hard to detect. Another possibility, that is not supported by the available neutron diffraction data, is that stacking faults result in a variation of the CF potential along the c axis. In this scenario, the level at 21 meV would be more strongly affected by such stacking faults given the strong charge density out of the plane for this eigenfunction (see SM [39] Fig. S4 for plots of the charge density for each

¹As explained in greater detail below, a constrained two-component Lorentzian has been used for the CF level at 21 meV.

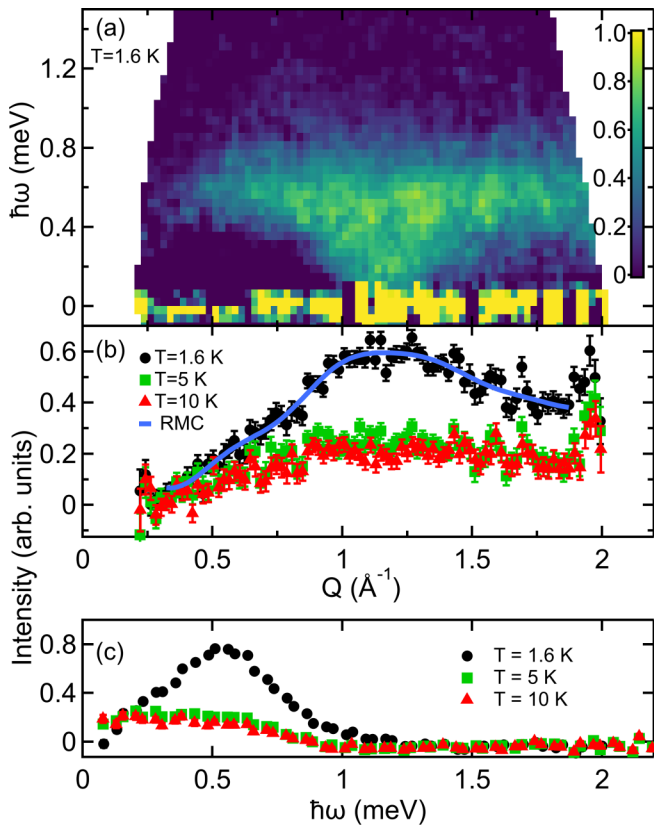


FIG. 4. Low-energy magnetic spectrum of YbCl_3 . All data have had the $T = 100$ K YbCl_3 measurement subtracted as a background. (a) Scattering intensity as a function of Q (top axis) and $\hbar\omega$. (b) Scattering intensity as a function of Q (top axis) integrated over $\hbar\omega = [0.1, 1.2]$ meV. The solid line is the RMC calculation described in the text. (c) Scattering intensity as a function of $\hbar\omega$ (bottom axis) integrated over $Q = [0.2, 2]$ \AA^{-1} .

eigenfunction). Additionally, first-principles calculations of the phonon density of states suggest that this feature is not the result of hybridization of the CF level with a nearby phonon mode. However, the symmetry of the closest phonon modes at 16 and 25 meV does not prohibit hybridization with the CF level [39]. Studies of single crystals are required to further understand the origin of this broadening. Finally, we note that using a single Lorentzian in the CF modeling does not significantly change the refined CF parameters.

To probe for low-energy magnetic correlations, we performed INS measurements using the HYSPEC instrument [59]. The same sample used in the SEQUOIA measurements was cooled to $T = 1.6, 5,$ and 10 K and measured with $E_i = 3.8$ meV at two positions of the detector bank to cover a large range of Q . A measurement at 100 K of the YbCl_3 sample was used as the background. Figure 4(a) shows the energy and wave-vector-dependent magnetic spectrum. A broad dispersive mode with additional scattering is evident. The additional scattering may be due to a quantum continuum, however, other explanations such as broadened excitations from a short-ranged ordered state, magnon decay, etc., cannot be excluded with the data at hand. The Q integrated scattering intensity in Fig. 4(c) shows a single peak at 0.5 meV with no indication of a spin gap within the energy resolution of 0.091 meV

or additional scattering intensity above 1.3 meV. Given that long-range magnetic order occurs at a maximum temperature of 0.6 K [37], the energy scale of the spin excitations suggests low-dimensional and/or frustrated spin interactions in YbCl_3 . The $\hbar\omega$ integrated intensity in Fig. 4(b) is a broad function which peaks at approximately $Q = 1.1$ \AA^{-1} likely corresponding to the reciprocal lattice points (110) and (020) , which is consistent with spin correlations within the basal plane. The data in Fig. 4(c) were collected at $T = 1.6$ K, which is at lower T than the maximum in the specific heat capacity (1.8 K) [37,39]. Thus, the low-temperature spin excitations may be responsible for a portion of the loss of entropy despite the lack of apparent long-range order. An additional observation is that the scattering observed here for YbCl_3 appears to be quite different from the scattering above the ordering temperature in polycrystalline samples of RuCl_3 [29] indicating the two materials have distinct spin Hamiltonians governing the physical behavior despite their structural and chemical similarities. Measurements using single crystals are required to fully understand the nature of the magnetic ground state and the spin excitation spectrum.

To investigate the spin-spin correlations in YbCl_3 , we performed reverse Monte Carlo (RMC) calculations as implemented in SPINVERT [60] (see SM [39] for more details). Within this approximation, we fit the integrated intensity of the low-energy excitation spectrum as a function of Q . Uniaxial, easy plane, and isotropic local spin anisotropies were all tried as initial starting points for the simulations. Only starting configurations with the spins in the plane resulted in good agreement with the data. The result of the RMC modeling with an easy plane anisotropy is shown as a solid line in Fig. 4(b). The radial spin-spin correlation function was calculated for each final spin configuration as a means to investigate the orientation of the spins with respect to each other. Assuming a purely hexagonal geometry, the nearest-neighbor spins are antiferromagnetically correlated, second-neighbor spins have weak ferromagnetic correlations, followed by a rapid decay of spin correlations at larger distances. This result is independent of the type of starting correlation used for the modeling.

We analyzed the spectroscopic properties of the quantum magnet YbCl_3 . Our studies show that YbCl_3 has CF excitations at $\hbar\omega = 21.04, 32.03,$ and 39.28 meV. The ground state is a well separated effective spin- $1/2$ doublet with easy plane anisotropy and an average magnetic moment of $2.24(5)\mu_B/\text{Yb}$. At $T = 1.6$ K, where long-range order is not believed to exist, the low-energy dynamics of YbCl_3 are consistent with an interacting spin system with antiferromagnetic nearest neighbor correlations.

We thank J. Liu for useful discussions. This work was supported by the US Department of Energy (DOE), Office of Science, Basic Energy Sciences, Materials Sciences and Engineering Division. This research used resources at the High Flux Isotope Reactor and Spallation Neutron Source, DOE Office of Science User Facilities operated by the Oak Ridge National Laboratory. The work of G.B.H. at ORNL was supported by Laboratory Director's Research and Development funds. The computing resources for VASP and INS simulations were made available through the VirtuES and the ICE-MAN projects, funded by Laboratory Directed Research

and Development program, as well as the Compute and Data Environment for Science (CADES) at ORNL. The US Government retains, and the publisher, by accepting the article for publication, acknowledges that the US Government retains a nonexclusive, paid-up, irrevocable, worldwide license to

publish or reproduce the published form of this manuscript, or allow others to do so, for US Government purposes. The Department of Energy will provide public access to these results of federally sponsored research in accordance with the DOE Public Access Plan [73].

-
- [1] L. Savary and L. Balents, *Rep. Prog. Phys.* **80**, 016502 (2016).
- [2] Y. Zhou, K. Kanoda, and T.-K. Ng, *Rev. Mod. Phys.* **89**, 025003 (2017).
- [3] H. Takagi, T. Takayama, G. Jackeli, G. Khaliullin, and S. E. Nagler, *Nat. Rev. Phys.* **1**, 264 (2019).
- [4] J. Knolle and R. Moessner, *Annu. Rev. Condens. Matter Phys.* **10**, 451 (2019).
- [5] K. A. Ross, Y. Qiu, J. R. D. Copley, H. A. Dabkowska, and B. D. Gaulin, *Phys. Rev. Lett.* **112**, 057201 (2014).
- [6] Y. Li, G. Chen, W. Tong, L. Pi, J. Liu, Z. Yang, X. Wang, and Q. Zhang, *Phys. Rev. Lett.* **115**, 167203 (2015).
- [7] J. A. M. Paddison, M. Daum, Z. Dun, G. Ehlers, Y. Liu, M. Stone, H. Zhou, and M. Mourigal, *Nat. Phys.* **13**, 117 (2016).
- [8] L. Balents, *Nature (London)* **464**, 199 (2010).
- [9] W. Witczak-Krempa, G. Chen, Y. B. Kim, and L. Balents, *Annu. Rev. Condens. Matter Phys.* **5**, 57 (2014).
- [10] J. G. Rau, E. K.-H. Lee, and H.-Y. Kee, *Annu. Rev. Condens. Matter Phys.* **7**, 195 (2016).
- [11] A. Kitaev, *Ann. Phys.* **321**, 2 (2006).
- [12] G. Jackeli and G. Khaliullin, *Phys. Rev. Lett.* **102**, 017205 (2009).
- [13] J. Chaloupka, G. Jackeli, and G. Khaliullin, *Phys. Rev. Lett.* **105**, 027204 (2010).
- [14] Y. Singh and P. Gegenwart, *Phys. Rev. B* **82**, 064412 (2010).
- [15] X. Liu, T. Berlijn, W.-G. Yin, W. Ku, A. Tsvelik, Y.-J. Kim, H. Gretarsson, Y. Singh, P. Gegenwart, and J. P. Hill, *Phys. Rev. B* **83**, 220403(R) (2011).
- [16] Y. Singh, S. Manni, J. Reuther, T. Berlijn, R. Thomale, W. Ku, S. Trebst, and P. Gegenwart, *Phys. Rev. Lett.* **108**, 127203 (2012).
- [17] S. K. Choi, R. Coldea, A. N. Kolmogorov, T. Lancaster, I. I. Mazin, S. J. Blundell, P. G. Radaelli, Y. Singh, P. Gegenwart, K. R. Choi *et al.*, *Phys. Rev. Lett.* **108**, 127204 (2012).
- [18] F. Ye, S. Chi, H. Cao, B. C. Chakoumakos, J. A. Fernandez-Baca, R. Custelcean, T. F. Qi, O. B. Korneta, and G. Cao, *Phys. Rev. B* **85**, 180403(R) (2012).
- [19] R. Comin, G. Levy, B. Ludbrook, Z.-H. Zhu, C. N. Veenstra, J. A. Rosen, Y. Singh, P. Gegenwart, D. Stricker, J. N. Hancock *et al.*, *Phys. Rev. Lett.* **109**, 266406 (2012).
- [20] S. Hwan Chun, J.-W. Kim, J. Kim, H. Zheng, C. C. Stoumpos, C. D. Malliakas, J. F. Mitchell, K. Mehlawat, Y. Singh, Y. Choi *et al.*, *Nat. Phys.* **11**, 462 (2015).
- [21] S. C. Williams, R. D. Johnson, F. Freund, S. Choi, A. Jesche, I. Kimchi, S. Manni, A. Bombardi, P. Manuel, P. Gegenwart *et al.*, *Phys. Rev. B* **93**, 195158 (2016).
- [22] K. Kitagawa, T. Takayama, Y. Matsumoto, A. Kato, R. Takano, Y. Kishimoto, R. Dinnebier, G. Jackeli, and H. Takagi, *Nature (London)* **554**, 341 (2018).
- [23] K. W. Plumb, J. P. Clancy, L. J. Sandilands, V. V. Shankar, Y. F. Hu, K. S. Burch, H.-Y. Kee, and Y.-J. Kim, *Phys. Rev. B* **90**, 041112(R) (2014).
- [24] L. J. Sandilands, Y. Tian, K. W. Plumb, Y.-J. Kim, and K. S. Burch, *Phys. Rev. Lett.* **114**, 147201 (2015).
- [25] J. A. Sears, M. Songvilay, K. W. Plumb, J. P. Clancy, Y. Qiu, Y. Zhao, D. Parshall, and Y.-J. Kim, *Phys. Rev. B* **91**, 144420 (2015).
- [26] M. Majumder, M. Schmidt, H. Rosner, A. A. Tsirlin, H. Yasuoka, and M. Baenitz, *Phys. Rev. B* **91**, 180401(R) (2015).
- [27] R. D. Johnson, S. C. Williams, A. A. Haghighirad, J. Singleton, V. Zapf, P. Manuel, I. I. Mazin, Y. Li, H. O. Jeschke, R. Valentí *et al.*, *Phys. Rev. B* **92**, 235119 (2015).
- [28] L. J. Sandilands, Y. Tian, A. A. Reijnders, H.-S. Kim, K. W. Plumb, Y.-J. Kim, H.-Y. Kee, and K. S. Burch, *Phys. Rev. B* **93**, 075144 (2016).
- [29] A. Banerjee, C. A. Bridges, J.-Q. Yan, A. A. Aczel, L. Li, M. B. Stone, G. E. Granroth, M. D. Lumsden, Y. Yiu, J. Knolle *et al.*, *Nat. Mater.* **15**, 733 (2016).
- [30] J. A. Sears, Y. Zhao, Z. Xu, J. W. Lynn, and Y.-J. Kim, *Phys. Rev. B* **95**, 180411(R) (2017).
- [31] A. Banerjee, J. Yan, J. Knolle, C. A. Bridges, M. B. Stone, M. D. Lumsden, D. G. Mandrus, D. A. Tennant, R. Moessner, and S. E. Nagler, *Science* **356**, 1055 (2017).
- [32] S.-H. Baek, S.-H. Do, K.-Y. Choi, Y. S. Kwon, A. U. B. Wolter, S. Nishimoto, J. van den Brink, and B. Büchner, *Phys. Rev. Lett.* **119**, 037201 (2017).
- [33] S.-H. Do, S.-Y. Park, J. Yoshitake, J. Nasu, Y. Motome, Y. S. Kwon, D. T. Adroja, D. J. Voneshen, K. Kim, T.-H. Jang *et al.*, *Nat. Phys.* **13**, 1079 (2017).
- [34] A. Banerjee, P. Lampen-Kelley, J. Knolle, C. Balz, A. A. Aczel, B. Winn, Y. Liu, D. Pajerowski, J. Yan, C. A. Bridges *et al.*, *npj Quantum Mater.* **3**, 8 (2018).
- [35] R. Hentrich, A. U. B. Wolter, X. Zotos, W. Brenig, D. Nowak, A. Isaeva, T. Doert, A. Banerjee, P. Lampen-Kelley, D. G. Mandrus *et al.*, *Phys. Rev. Lett.* **120**, 117204 (2018).
- [36] Y. Kasahara, T. Ohnishi, Y. Mizukami, O. Tanaka, S. Ma, K. Sugii, N. Kurita, H. Tanaka, J. Nasu, Y. Motome *et al.*, *Nature (London)* **559**, 227 (2018).
- [37] J. Xing, H. Cao, E. Emmanouilidou, C. Hu, J. Liu, D. Graf, A. P. Ramirez, G. Chen, and N. Ni, [arXiv:1903.03615](https://arxiv.org/abs/1903.03615).
- [38] Z.-X. Luo and G. Chen, [arXiv:1903.02530](https://arxiv.org/abs/1903.02530).
- [39] See Supplemental Material at <http://link.aps.org/supplemental/10.1103/PhysRevB.100.180406> for additional details, which includes Refs. [61–72].
- [40] J. G. Rau, L. S. Wu, A. F. May, L. Poudel, B. Winn, V. O. Garlea, A. Huq, P. Whitfield, A. E. Taylor, M. D. Lumsden *et al.*, *Phys. Rev. Lett.* **116**, 257204 (2016).
- [41] T. Haku, K. Kimura, Y. Matsumoto, M. Soda, M. Sera, D. Yu, R. A. Mole, T. Takeuchi, S. Nakatsuji, Y. Kono, T. Sakakibara, L. J. Chang, and T. Masuda, *Phys. Rev. B* **93**, 220407(R) (2016).

- [42] S.-Y. Park, S.-H. Do, K.-Y. Choi, J.-H. Kang, D. Jang, B. Schmidt, M. Brando, B.-H. Kim, D.-H. Kim, N. P. Butch *et al.*, *Nat. Commun.* **7**, 12912 (2016).
- [43] J. G. Rau, L. S. Wu, A. F. May, A. E. Taylor, I.-L. Liu, J. Higgins, N. P. Butch, K. A. Ross, H. S. Nair, M. D. Lumsden *et al.*, *J. Phys.: Condens. Matter* **30**, 455801 (2018).
- [44] L. S. Wu, W. J. Gannon, I. A. Zaliznyak, A. M. Tselik, M. Brockmann, J.-S. Caux, M. S. Kim, Y. Qiu, J. R. D. Copley, G. Ehlers *et al.*, *Science* **352**, 1206 (2016).
- [45] L. S. Wu, S. E. Nikitin, Z. Wang, W. Zhu, C. D. Batista, A. M. Tselik, A. M. Samarakoon, D. A. Tennant, M. Brando, L. Vasylychko *et al.*, *Nat. Commun.* **10**, 698 (2019).
- [46] J. G. Rau and M. J. P. Gingras, *Phys. Rev. B* **98**, 054408 (2018).
- [47] G. E. Granroth, A. I. Kolesnikov, T. E. Sherline, J. P. Clancy, K. A. Ross, J. P. C. Ruff, B. D. Gaulin, and S. E. Nagler, *J. Phys.: Conf. Ser.* **251**, 012058 (2010).
- [48] M. Kresch, M. Lucas, O. Delaire, J. Y. Y. Lin, and B. Fultz, *Phys. Rev. B* **77**, 024301 (2008).
- [49] R. T. Azuah, L. R. Kneller, Y. Qiu, P. L. W. Tregenna-Piggott, C. M. Brown, J. R. D. Copley, and R. M. Dimeo, *J. Res. Natl. Inst. Stand. Technol.* **114**, 341 (2009).
- [50] O. Arnold, J. Bilheux, J. Borreguero, A. Buts, S. Campbell, L. Chapon, M. Doucet, N. Draper, R. F. Leal, M. Gigg *et al.*, *Nucl. Instrum. Methods Phys. Res., Sect. A* **764**, 156 (2014).
- [51] B. G. Wybourne, *Spectroscopic Properties of Rare Earths* (Wiley, New York, 1965).
- [52] B. R. Judd, *Proc. Phys. Soc. London, Sect. A* **69**, 157 (1956).
- [53] B. R. Judd, *Proc. Phys. Soc.* **74**, 330 (1959).
- [54] K. W. H. Stevens, *Proc. Phys. Soc. London, Sect. A* **65**, 209 (1952).
- [55] U. Walter, *J. Phys. Chem. Solids* **45**, 401 (1984).
- [56] J. L. Prather, National Bureau of Standards Monograph (US) 19, 1961, <https://nvlpubs.nist.gov/nistpubs/Legacy/MONO/nbsmonograph19.pdf>.
- [57] C. Kittel, *Introduction to Solid State Physics*, 8th ed. (Wiley, Hoboken, NJ, 2005).
- [58] M. T. Hutchings, *Solid State Phys.* **16**, 227 (1964).
- [59] B. Winn, U. Filges, V. O. Garlea, M. Graves-Brook, M. Hagen, C. Jiang, M. Kenzelmann, L. Passell, S. M. Shapiro, X. Tong *et al.*, *EPJ Web Conf.* **83**, 03017 (2015).
- [60] J. A. M. Paddison, J. R. Stewart, and A. L. Goodwin, *J. Phys.: Condens. Matter* **25**, 454220 (2013).
- [61] A. Huq, J. P. Hodges, L. Heroux, and O. Gourdon, *Z. Kristallogr. Proc.* **1**, 127 (2011).
- [62] B. H. Toby and R. B. Von Dreele, *J. Appl. Crystallogr.* **46**, 544 (2013).
- [63] U. Walter, *Z. Phys. B* **62**, 299 (1986).
- [64] G. Kresse and J. Furthmüller, *Phys. Rev. B* **54**, 11169 (1996).
- [65] G. Kresse and D. Joubert, *Phys. Rev. B* **59**, 1758 (1999).
- [66] P. E. Blöchl, *Phys. Rev. B* **50**, 17953 (1994).
- [67] J. P. Perdew, K. Burke, and M. Ernzerhof, *Phys. Rev. Lett.* **77**, 3865 (1996).
- [68] H. Jiang, P. Rinke, and M. Scheffler, *Phys. Rev. B* **86**, 125115 (2012).
- [69] J. Klimeš, D. R. Bowler, and A. Michaelides, *J. Phys.: Condens. Matter* **22**, 022201 (2009).
- [70] I. T. A Togo, *Scr. Mater.* **108**, 1 (2015).
- [71] X. Gonze and C. Lee, *Phys. Rev. B* **55**, 10355 (1997).
- [72] Y. Q. Cheng, L. L. Daemen, A. I. Kolesnikov, and A. J. Ramirez-Cuesta, *J. Chem. Theory Comput.* **15**, 1974 (2019).
- [73] <http://energy.gov/downloads/doe-public-access-plan>.